J. Fluid Mech. (1998), *vol.* 359, *pp.* 357–381. Printed in the United Kingdom

The effects of a favourable pressure gradient and of the Reynolds number on an incompressible axisymmetric turbulent boundary layer. Part 2. The boundary layer with relaminarization

By D. WARNACK AND H. H. FERNHOLZ

Hermann-Föttinger-Institut für Strömungsmechanik, Technische Universität Berlin, Strasse des 17. Juni 135, 10623 Berlin, Germany

(Received 21 June 1996 and in revised form 4 November 1997)

This is an experimental investigation of two turbulent boundary layers (cases 2 and 4) where the streamwise negative pressure gradient changes mean properties of the flow, e.g. mean velocity profiles and skin friction, so that they display laminar-like behaviour. The maximum acceleration parameter $K \leqslant 4 \times 10^{-6}$ and the starting value of the Reynolds number is 862 or 2564. Relaminarization occurs in both boundary layers as a gradual change of the turbulence properties and is not catastrophic. Retransition, however, is a fast process due to the remaining turbulence structure and may be compared with bypass transition. Together with an extensive investigation of the turbulence structure as in the companion paper, Part 1, which describes two cases (1 and 3) of boundary layers which remain turbulent, spectra and integral length scales for all four boundary layers are discussed.

1. Introduction

Sternberg (1954) reported for the first time that a supersonic fully turbulent boundary layer reverted to a laminar-like state when it was subjected to a Prandtl–Meyer expansion, i.e. to a high acceleration. Several investigators have since performed experiments on subsonic flows (e.g. Launder 1964; Patel & Head 1968; Badri Narayanan & Ramjee 1969; Blackwelder & Kovasznay 1972) and confirmed 'relaminarization'. Excellent review articles covering flows with relaminarization were given by Narasimha & Sreenivasan (1973, 1979) and by Sreenivasan (1982). As an example of a more recent investigation we mention Ichimiya (1995). In Part 1 (Fernholz & Warnack 1998) two cases (1 and 3) of boundary layers maintained in the fully turbulent state are described in detail. Here, cases 2 and 4, which include relaminarization, are discussed.

From among the three archetypes of reverting flows suggested by Narasimha (1977, 1983) "the third class of these flows is exemplified by a turbulent boundary layer subjected to severe acceleration. Reversion here is not so much the result of dissipation or destruction of energy (although these mechanisms are also operating), but rather of the domination of pressure forces over slowly responding Reynolds stresses in the outer region, accompanied by the generation of a new laminar 'subboundary' layer stabilized by the acceleration."

This statement sets the scene for the discussion of the present experimental results

	$K_{\max} \times 10^6$	$Re_{\delta_2 S}$	H_{12S}	$Re_{\delta_2 \min}$	$H_{12\min}$	$H_{12\max}$	$Re_{\delta_2 E}$	H_{12E}
Case 2	4.0	862	1.48	357	1.34	1.68	1399	1.40
Case 4	3.88	2564	1.42	649	1.26	1.60	1532	1.38
BN–R 2	≈ 8.1	≈ 300	≈ 1.5	≈ 130	≈ 1.36	2.6	≈ 300	≈ 2.6
BN–R 3	≈ 8.1	≈ 400	≈ 1.35	≈ 130	≈ 1.36	2.0	≈ 250	≈ 2.0
Launder (1964)	—	336	1.63	155	1.59	2.4	298	2.38
Launder (1964)	≈ 1.8	874	1.42	498	1.38	1.8	498	1.8

TABLE 1. Boundary layer parameters. Here we have used the same parameters and indices as in table 1 of Part 1. BN–R 2 and BN–R 3 denote cases 2 and 3 of Badri Narayanan & Ramjee (1969)

and gives rise to several questions, such as the conditions for the onset of 'relaminarization', the behaviour of the boundary layer during its laminar-like state, and its reversion to the turbulent state.

There appears to be unanimous agreement that a turbulent boundary layer must be severely accelerated, say have an acceleration parameter $K > 3 \times 10^{-6}$, before it becomes laminar-like and that the extent of the laminar-like region in the boundary layer gets larger the smaller the Reynolds number. Therefore the early experiments (see table 1 of Part 1) and especially those of Badri Narayanan & Ramjee (1969) had initial Reynolds numbers Re_{δ_2} of 306 and 406, respectively, which were so small, however, that low-Reynolds-number effects could not be excluded. The initial Re_{δ_2} for cases 2 and 4 of the present experimental investigation were therefore chosen to be much higher (862 and 2564). Case 4 has starting conditions ($Re_{\delta_2} = 2564$ and $H_{12} = 1.42$) which are very similar to the boundary layer investigated by Blackwelder & Kovasznay (1972) where, however, the maximum acceleration parameter K was higher, 4.8×10^{-6} as compared with 3.88×10^{-6} in case 4.

The c_f, Re_{δ_2} plot (figure 1) presents cases 2 and 4 as well as BN & R flows 2 and 3 (classified as reliable by Sreenivasan 1982). All these boundary layer flows show a behaviour different from that of cases 1 and 3 (figure 1 of Part 1) in that the c_f-values obtained are much lower, an indication of the laminar-like state of the mean flow of the boundary layer. It would, of course, be helpful to have a criterion indicating when a boundary layer reverts to the laminar-like state. A detailed discussion of parameters which may serve as a criterion was provided by Narasimha & Sreenivasan (1973) and later updated by Sreenivasan (1982). As in the case of the departure of the mean-velocity profile from the standard log law, we agree with the statement of Narasimha & Sreenivasan (1973) that 'relaminarization is not catastrophic and that for this reason no satisfactory criterion for its occurence has yet been given'. 'Relaminarization' by a favourable pressure gradient (FPG) does not show a 'switchoff' of turbulent energy production but a gradual change-over to laminar-like mean-velocity profiles and skin-friction values (classified as hard laminarization by Narasimha 1983).

There are, however, changes of various quantities which might indicate such a reversion to a laminar-like state. These quantities are best non-dimensionalized by inner-law scales, the skin-friction velocity u_τ and the length scale ν/u_τ, which can only be determined from reliable wall shear stress data. The measuring techniques for skin friction must be applicable in turbulent, transitional, and laminar-like boundary layers (see the discussion in section 2 of Part 1) and the mean skin friction, its fluctuating value and its higher moments provide insight into the different states of the FPG boundary layer during the stages of small and high acceleration, of laminar-like behaviour, and during reversion to turbulent flow.

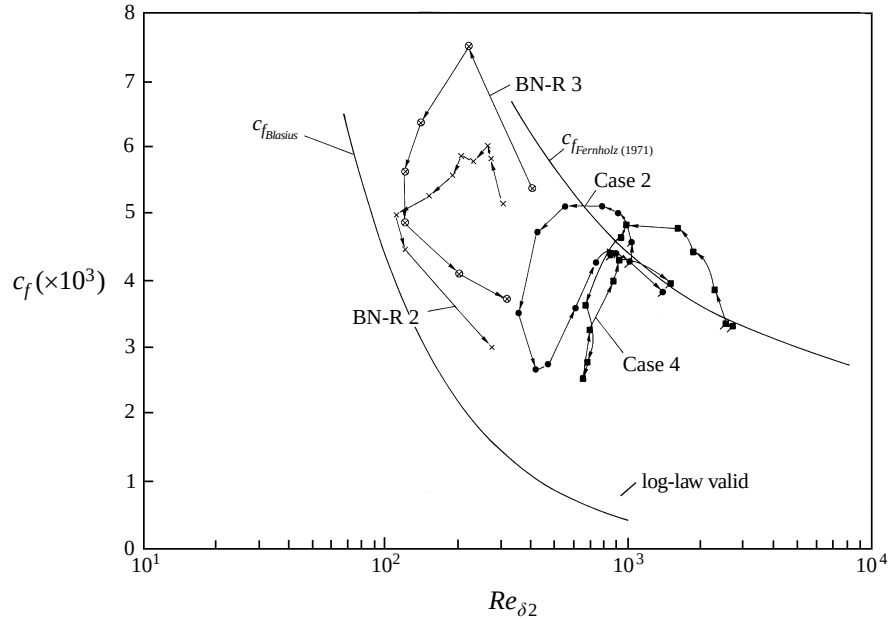

FIGURE 1. The (c_f, Re_{δ_2})-plane for FPG boundary layers with relaminarization (cases 2 and 4, present experiment; Badri Narayanan & Ramjee 1969, BN–R).

As in Part 1 we shall discuss first the mean-flow quantities and then the turbulence. For the experimental set-up and the measuring techniques the reader is referred to Part 1.

2. Discussion of the mean-flow data

Figure 2 shows the distribution of the boundary layer thickness δ non-dimensionalized by δ_0 at a reference station in the zero pressure gradient (ZPG) region. The dominant quantity responsible for the development of δ/δ_0 is the pressure gradient which is characterized here by the shape parameter $m = (x\mathrm{d}\bar{u}/\mathrm{d}x)/u_\delta$ in the Falkner–Skan equation. Like similar laminar boundary layers (e.g. Loitsianski 1972) the boundary thickness in the flow direction rises when $m < 1$ and falls when $m > 1$.

Since the decrease of the momentum loss thickness δ_2 is larger than the rise of u_δ, Re_{δ_2} decreases in regions with high acceleration. This is shown in figures 3 and 4 where we present the streamwise development of the acceleration parameter K with $K_{\max} \approx 4 \times 10^{-6}$, the skin-friction coefficient c_f, the Reynolds number Re_{δ_2}, and the shape parameter H_{12}. Since the same centre body was used to generate the pressure distribution the streamwise distributions of K are similar. The initial Reynolds number differed, however, by a factor of 3 between cases 2 and 4.

Re_{δ_2} reacts first to the acceleration and falls from a maximum (1045 and 2574) to a minimum value of 357 and 649, respectively. Following the pattern of a fully turbulent accelerated boundary in the entry region, the skin-friction coefficient rises to its first peak and H_{12} decreases to its respective minimum value (1.34 and 1.26) with $c_{f\max}$ and $H_{12\min}$ coinciding approximately with the maximum of K. Downstream of this peak the interaction between the mean-velocity distribution and the turbulence structure changes strongly, since the mean velocity profiles develop a laminar-like

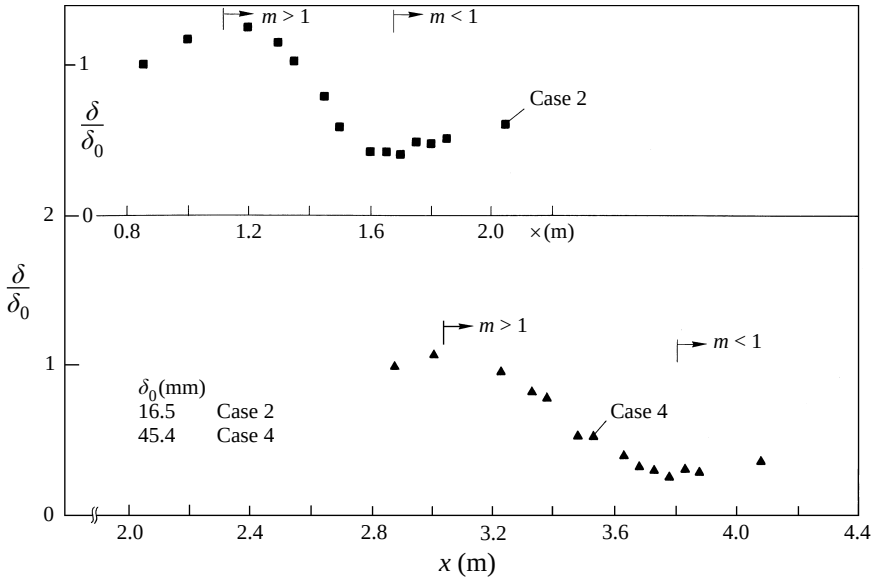

FIGURE 2. Development of the boundary layer thickness in the streamwise direction in a FPG boundary layer (cases 2 and 4).

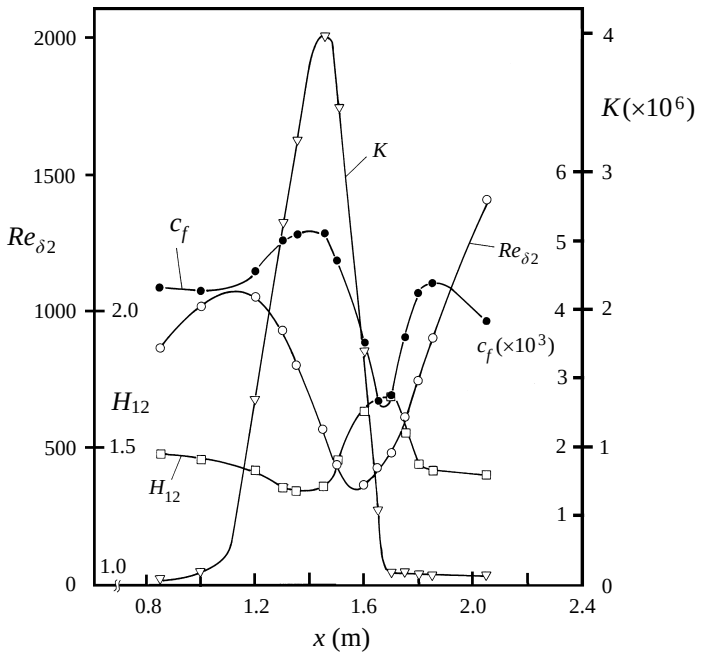

FIGURE 3. Streamwise development of the Reynolds number Re_{δ_2}, the shape parameter H_{12}, the skin-friction coefficient c_f, and the acceleration parameter K in a FPG boundary layer with relaminarization. Case 2 (lines are for visual aid only).

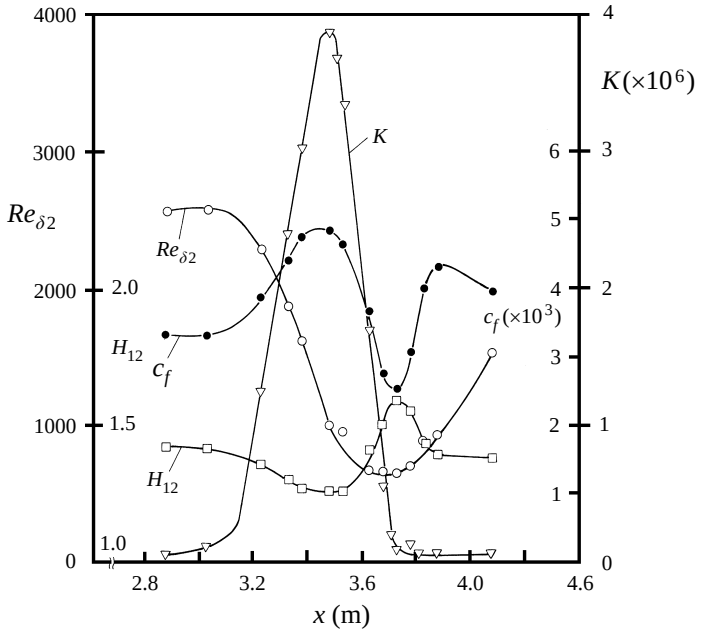

FIGURE 4. As figure 3 but for case 4.

shape independent of the still strong turbulence (e.g. figure 5). This process is accompanied by a rise of the shape parameter H_{12} to its respective maximum value (1.68 and 1.60) at the end of the acceleration region. These values are lower than $H_{12\,\max} = 1.78$ as measured by Blackwelder & Kovasznay (1972) where $K_{\max}(4.8 \times 10^{-6})$ was higher, but in both cases the mean-velocity profiles show a distinct laminar-like behaviour (see e.g. figure 9). At the end of the acceleration region the interaction between the mean velocity profile and the turbulence structure is reactivated and the shape parameter H_{12} falls to a value which is characteristic of a ZPG turbulent boundary layer profile.

The process towards a laminar-like mean velocity profile is accompanied by a sharp fall in c_f which begins at the location of the minimum of H_{12} and ends at its maximum, reflecting the large difference in c_f between a turbulent and a laminar-like boundary layer (see figure 1). The retransition towards a turbulent boundary layer then leads to an increase of the skin-friction coefficient c_f.

As a comparison with cases 1 and 3 (Part 1), the distance from the location of $Re_{\delta_2\,\min}$ to the last measuring station was $66\delta_{0\min}$ and $26\delta_{0\min}$ for cases 2 and 4, respectively. The corresponding lengths of the acceleration region were $36\delta_{0s}$ and $19\delta_{0s}$.

The mean velocity profiles in inner-law scaling for cases 2 and 4 are shown in figures 5 and 6, respectively. Initially, they pass through the same stages as the fully turbulent cases 1 and 3 (see Part 1) and their departure from the standard log law (cf. Patel & Head 1968; Badri Narayanan & Ramjee 1969) is accompanied by the same changes in physical properties as described in § 3 of Part 1. The main difference between the fully turbulent and the laminar-like FPG boundary layer is the larger departure of the mean profiles from the standard log law in the laminar-like boundary layer. The profile with the largest departure (⧅ in both cases) is that for which H_{12} has its maximum and c_f its minimum value. At this position one also finds maxima of two higher moments of the fluctuating skin friction, the skewness $S_{\tau_w'}$ and the

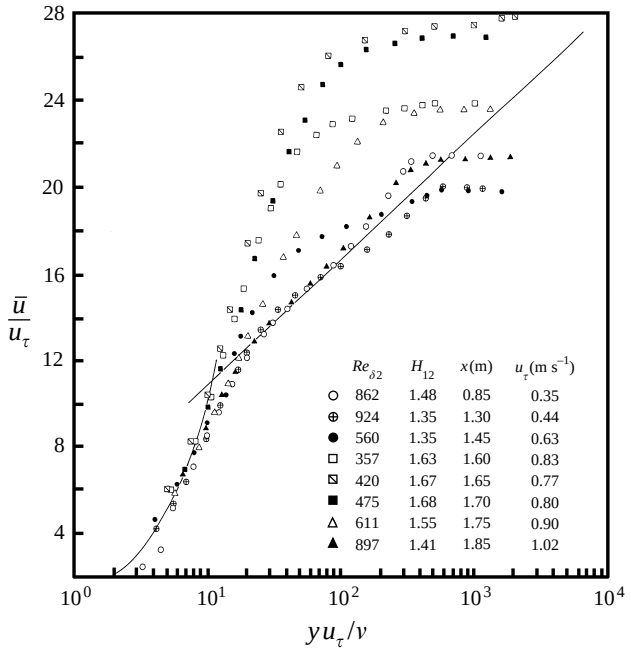

FIGURE 5. Profiles of the mean velocity in inner-law scaling in a FPG turbulent boundary layer with 'relaminarization'. Case 2.

flatness $F_{\tau_w'}$. The streamwise distributions of $Tu_{\tau_w'} = (\overline{\tau_w'^2})^{1/2}/\tau_w$ and of the skewness and flatness of the fluctuating value of the skin friction τ_w', as measured by a wall hot wire, are shown in figures 7 and 29† for cases 2 and 4. At $x = 1.65$ m (where $H_{12} = 1.67$, case 2) the skewness is increased by approximately a factor of 3 and the flatness by a factor of 4 which is much higher than in the fully turbulent FPG boundary layer of case 1 (figure 8 of Part 1). The high values of $F_{\tau_w'}$ (for cases 2 and 4) indicate large velocity spikes within the flow at the wall. This is confirmed by the time series of the instantaneous wall shear stress (figure 8) just downstream of $K_{\max}$ at $x = 1.65$ m which is compared with that in the fully turbulent ($x = 0.85$ m and 2.05 m) boundary layer region (see also the comments concerning the flatness $F_{\tau_w'}$ in figure 20 of Part 1). The spikes are indicators of the reappearance of high-frequency turbulent bursts superimposed on the relatively low-frequency residual turbulence as discussed by Launder (1964).

Returning to the measured mean-velocity profiles in the laminar-like state, it is appropriate to compare them with calculated laminar profiles at the same shape parameter and Re_{δ_2}. The comparison (figure 9) shows that the agreement between measured and calculated profiles grows with increasing values of H_{12} (see the legend in figure 5) and can be explained by the decreasing strength of the interaction between the turbulence and the mean-velocity distribution which is caused by the waning turbulence level in the outer region of the laminar-like boundary layer (for the turbulence quantities see § 3).

† For reasons of space limits figures 29 to 32 are in a separate annex available from the JFM Editorial Office.

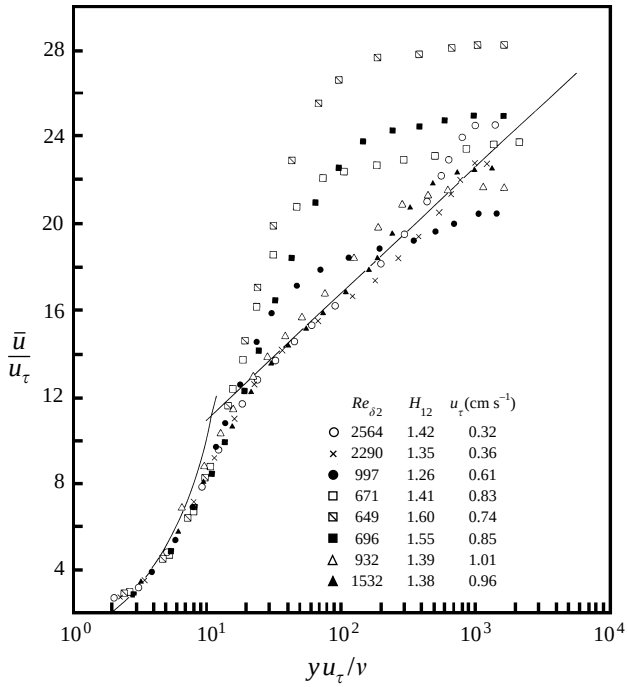

FIGURE 6. As figure 5 but for case 4.

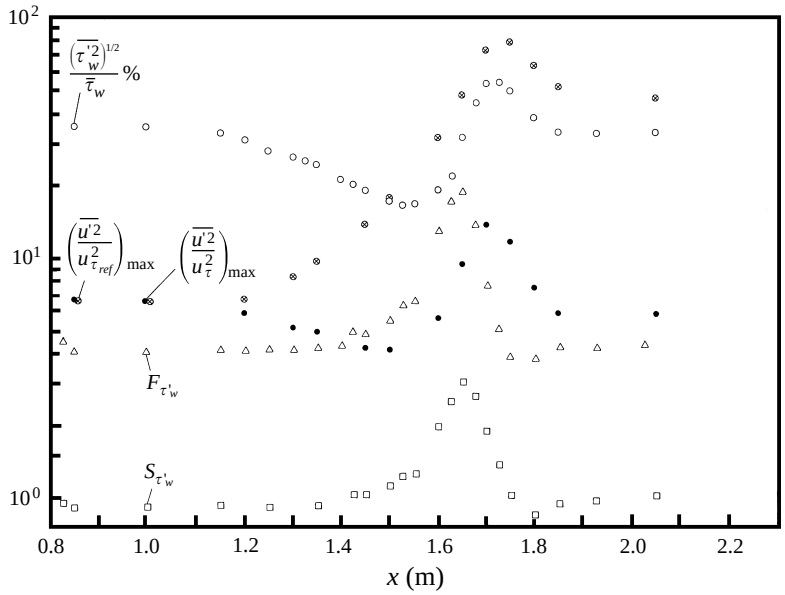

FIGURE 7. Streamwise development of the skin-friction fluctuation, the skewness $S_{\tau'_w}$ and flatness $F_{\tau'_w}$, and the maximum value of the dimensionless Reynolds normal-stress component $(\overline{u'^2}/u^2_\tau)_{\max}$ in a turbulent boundary layer with a strong favourable pressure gradient and 'relaminarization'. Case 2.

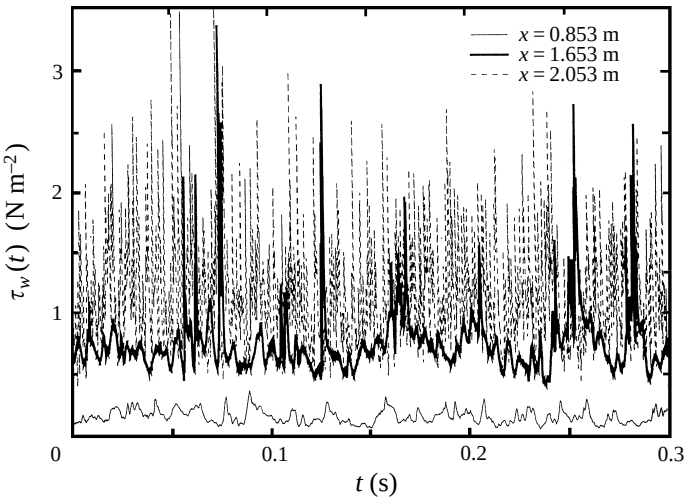

FIGURE 8. Time record of the wall shear stress (wall hot wire). Case 2.

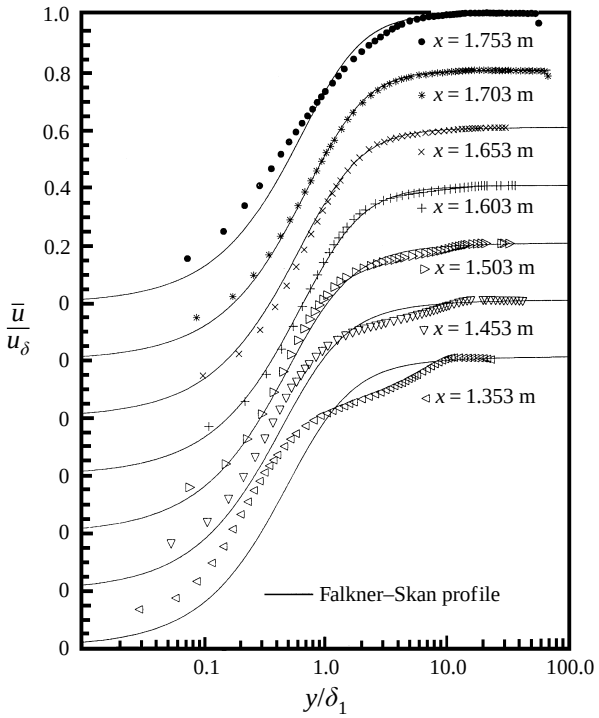

FIGURE 9. Comparison of measured mean-velocity profiles in a FPG boundary layer with Falkner–Skan profiles at the same H_{32} and Re_{δ_2}. Case 2.

3. Discussion of the turbulence data

The three Reynolds normal stress profiles (case 2) of the canonical boundary layer ($x = 0.85$ m, $H_{12} = 1,47$, $Re_{\delta_2} = 862$), scaled on the local skin-friction velocity, are compared with those close to the H_{12} peak and the c_f minimum of the laminar-like boundary layer ($x = 1.70$ m, $H_{12} = 1.68$, $Re_{\delta_2} = 475$) in figure 10. The absolute

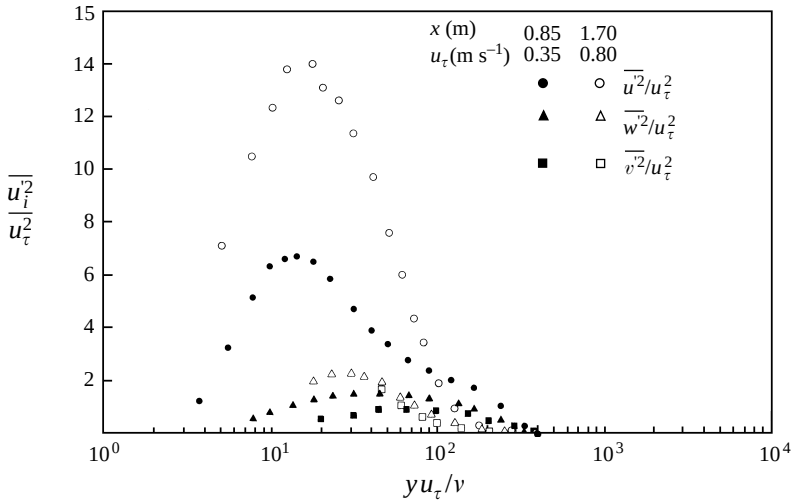

FIGURE 10. Profiles of the Reynolds normal stresses at the first measuring station and at the occurrence of the maximum values ($x = 1.70$) of the Reynolds normal stresses in a FPG turbulent boundary layer with 'relaminarization'. Case 2.

level of the Reynolds normal stresses, especially $\overline{\rho u'^2}$ and $\overline{\rho v'^2}$, in the near-wall region ($y^+ \lesssim 80$), increases much more strongly than u_τ which rises by approximately a factor 2. In the outer region the profiles in the laminar-like flow lie below those in the ZPG boundary layer.

The development of the largest component, $\overline{\rho u'^2}$, in the streamwise direction is shown in absolute terms, i.e. non-dimensionalized by $u^2_{\tau\ ref}$, in figure 11. $\overline{\rho u'^2}$ increases by about a factor of 10 at $y/\delta = 0.5$ between the initial ($\circ$) and the last measured profile ($\times$). This is a larger increase than for the fully turbulent boundary layer where the factor is only 4 (figure 10 of Part 1) and larger than found by Blackwelder & Kovasznay (1972). Figure 12, where the local skin-friction velocity is used for scaling, shows that the profile with the relative peak value occurs at the location where H_{12} reaches its maximum and c_f its minimum. The same trend may be observed for the $\overline{\rho u'^2}$-profiles of case 4 where the initial Reynolds number is higher (figure 30).

The location $y^+_{\max}$ of the peak value of $\overline{u'^2}/u_\tau^2$ in both cases shows only little variation as we have seen already for cases 1 and 3. The range is $12 \leqslant y^+_{\max} \leqslant 14$ for the canonical and the small-FPG boundary layers and $17 \leqslant y^+_{\max} \leqslant 24$ for the highly accelerated laminar-like regions of cases 2 and 4. This indicates an increase of the thickness of the near-wall layer (viscous sublayer and buffer layer) in the laminar-like region. The FPG $\overline{u'^2}/u_\tau^2$-profiles show no self-similarity in the near-wall region as found for the canonical boundary layer (Fernholz & Finley 1996). The peak value of $\overline{u'^2}/u_\tau^2$ increases until $H_{12\max}$ is reached and then falls showing an undershoot for the last profile ($\blacktriangle$) in cases 2 and 4. This undershoot is probably not physical but a hot-wire effect due to the influence of the relatively high value of ℓ^+ ($= \ell u_\tau/\nu$ where ℓ is the active wire length).

Figure 13 shows the Reynolds shear stress profiles plotted against y/δ for case 2 (no X-wire data for case 4 are available). They are made dimensionless by $u^2_{\tau,\ ref}$ and present the absolute changes of the Reynolds shear stress. Downstream of the last ZPG profile ($\bullet$) the level of the profiles ($\square, \boxtimes$) begins to rise first in the inner region and then in the outer region, to the profile with $H_{12\ \max}$ ($\blacksquare$) and beyond into the

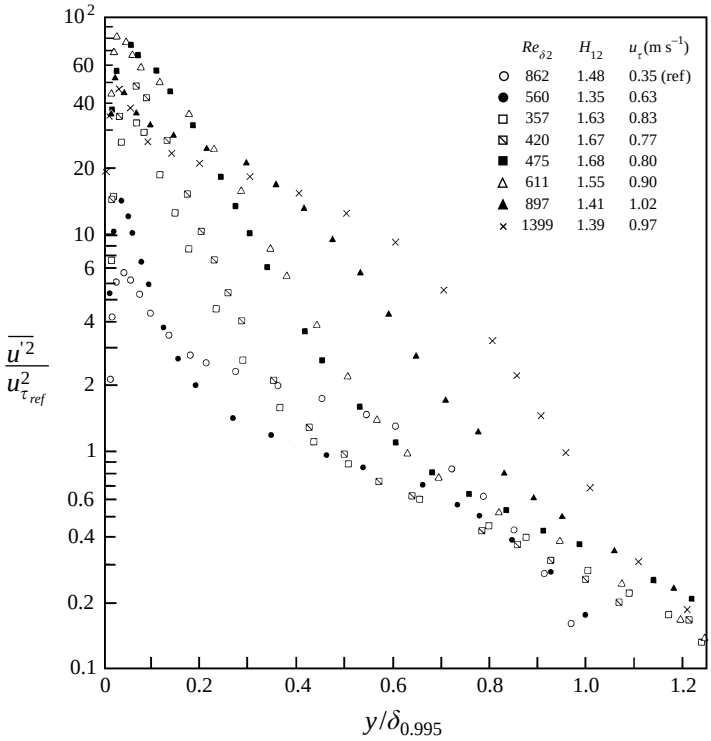

FIGURE 11. Profiles of the Reynolds normal stress component $\overline{\rho u'^2}$ in a FPG turbulent boundary layer with 'relaminarization' (non-dimensionalized by $\overline{\rho} u_{\tau\ ref}$). Case 2.

relaxation region (▲, ×) of the boundary layer. This trend is similar to the behaviour of the Reynolds shear-stress profiles in case 1 (figure 12 of Part 1) but differs in that the growth of the shear stress extends further out into the boundary layer than for the 'fully turbulent' case 1.

Figure 14 shows the profiles of the total, the Reynolds shear, and the molecular shear stress at the same streamwise position as the Reynolds normal stresses in figure 10. Here the large difference between the profiles at the two positions is caused partly by the strong increase of $\overline{\tau}_w$ and partly by the weaker increase of $\overline{\rho u'v'}$. The data close to the wall in figure 14 and the Reynolds shear stresses (in figure 15) were calculated by extrapolation as described in Part 1.

The initial Reynolds shear stress profile (○, ZPG) compares well with the low-Reynolds-number measurements of Erm (1988) and a DNS of J. G. Brasseur (1994, personal communication) at about the same Re_{δ_2} as shown by Fernholz & Finley (1996). Owing to the subsequent acceleration $\overline{\tau}_w$ rises much faster than $|\overline{\rho u'v'}|$ which leads to a sharp fall of $(-\overline{u'v'}/u_\tau^2)_{\max}$ from 0.72 (○) to 0.29 (●). Downstream of the minimum Reynolds number (□) the Reynolds shear stress increases more strongly than $\overline{\tau}_w$ until a peak value of $(-\overline{u'v'}/u_\tau^2) \approx 0.90$ is reached which is again typical for a ZPG turbulent boundary layer. Qualitatively the development of the Reynolds shear stress profiles in a FPG laminar-like and a fully turbulent boundary layer is similar. What is different, however, is the growth of the Reynolds shear stress in the outer region of the boundary layer, which lags behind the skin friction and the near-wall molecular shear stress.

A comparison between figures 15 and 12 reveals that downstream from the location

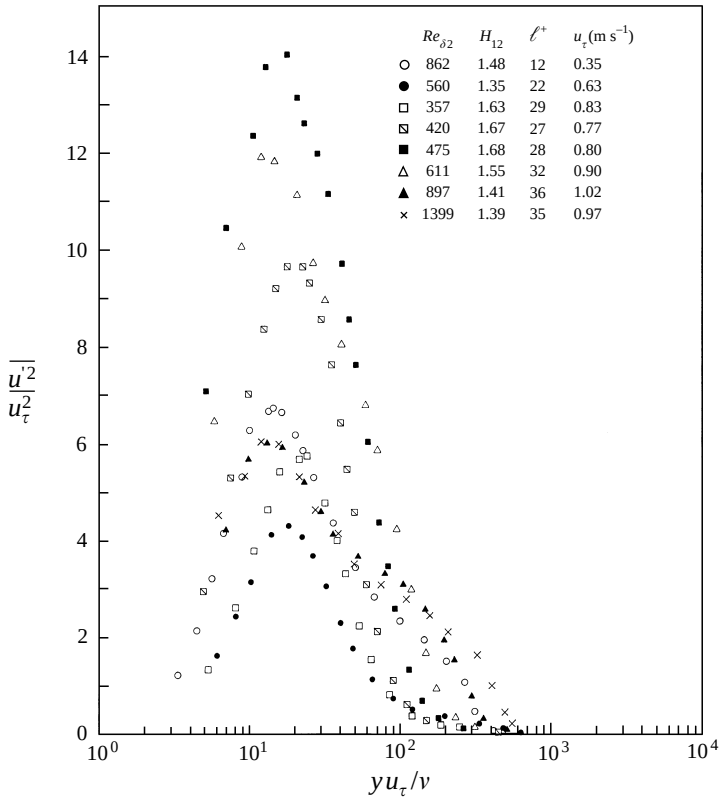

FIGURE 12. Profiles of the Reynolds normal-stress component $\overline{\rho}\overline{u'^2}$ scaled by the local skin-friction velocity in a FPG turbulent boundary layer with 'relaminarization' (case 2).

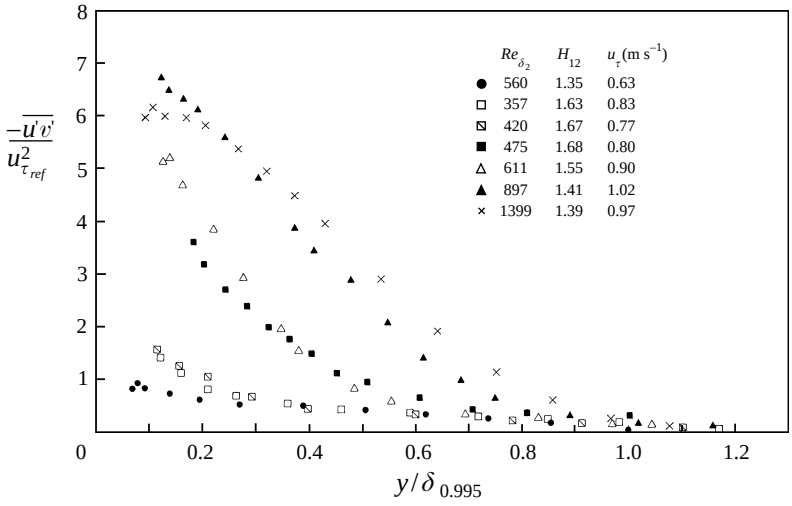

FIGURE 13. Profiles of the Reynolds shear stress component $\overline{\rho}\overline{u'v'}$ in a FPG turbulent boundary layer (non-dimensionalized by $u_{\tau_{ref}}$) with 'relaminarization'. Case 2.

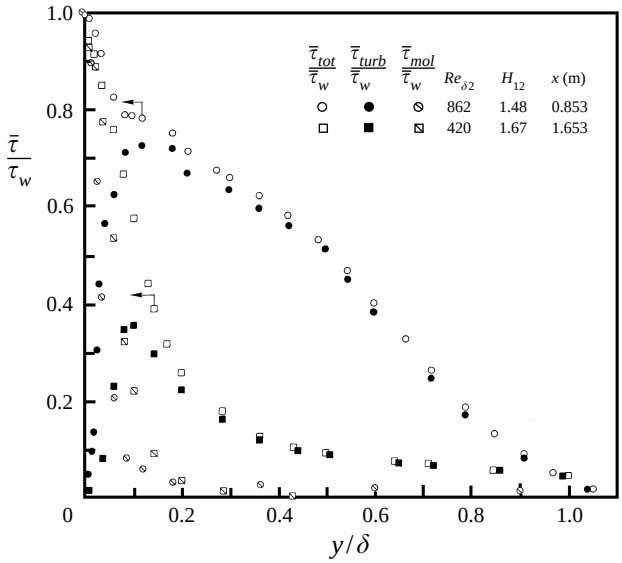

FIGURE 14. Distribution of the total, the molecular, and the Reynolds shear stress at two positions in a FPG boundary layer with 'relaminarization' (case 2). ← Data extrapolated.

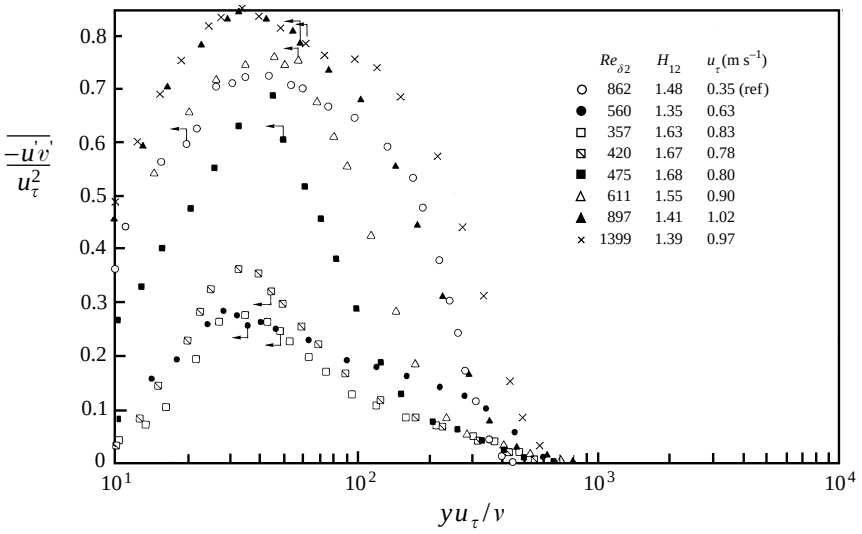

FIGURE 15. Profiles of the Reynolds shear stress component $\overline{\rho u'v'}$ in a FPG boundary layer with 'relaminarization'. Case 2. ← Data extrapolated.

of the minimum Reynolds number ($Re_{\delta_2} = 357$; □) the $\overline{\rho u'^2}$-component increases much faster than $\overline{\rho}|\overline{u'v'}|$ and falls again to its ZPG value after it has passed through an overshoot, whereas $\overline{\rho}|\overline{u'v'}|$ increases steadily finally to reach its ZPG value, here, of course, at a larger Re_{δ_2} than the initial profile.

The development of the $\overline{\rho u'^2}$- and $\overline{\rho u'v'}$-profiles is determined mainly by the respective turbulence production. The production terms are made dimensionless by ν/u_τ^4 and shown in figure 16. The two ZPG-profiles at the start (○) and at the end (×)

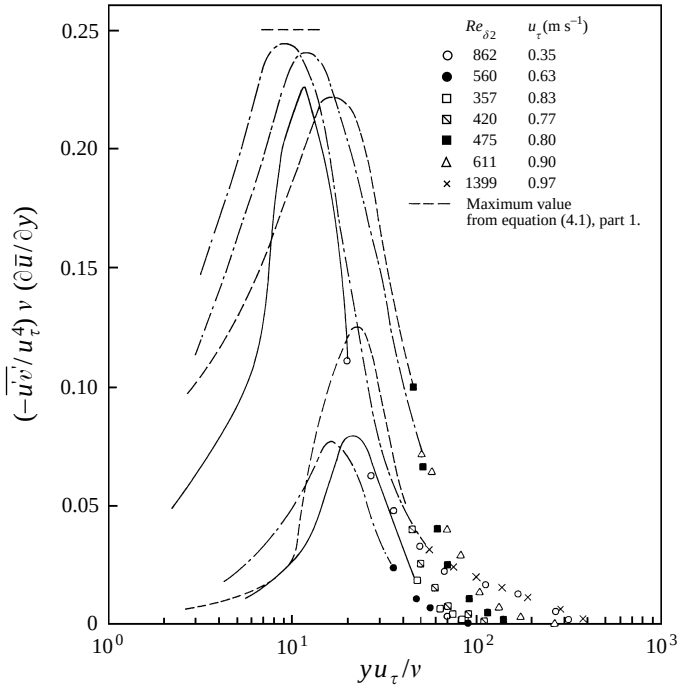

FIGURE 16. Distribution of the production term for the turbulent kinetic energy in a FPG turbulent boundary layer with 'relaminarization'. Case 2 (lines denote extrapolated data).

of the boundary layer reach exactly the peak values (denoted by - - -) predicted by equation (4.1) of Part 1 within 10 %.

This is a satisfactory check for the reliability of the measurements and the interpolation procedure. The production minimum corresponds with the position of $Re_{\delta_2 \min}$ which is downstream of the lowest profile of $\overline{\rho}\overline{u'^2}$ (•, figure 12). The production does not show the overshoot of the Reynolds normal stress profiles but follows much more closely the development of the Reynolds shear stress profiles which are influenced by the production profiles $\overline{v'^2}\delta_1(\partial\bar{u}/\partial y)/u_\tau^3$. These are shown in figure 31 but do not provide maximum values since they could not be extrapolated towards the wall and therefore do not allow conclusions in this region except that the largest reduction of the production occurs between the two profiles (○, •) at $Re_{\delta_2} = 862$ and 560.

Higher moments of the fluctuating velocities u', v' and w' were measured but we show only profiles of the skewness $S_{u'}$ and of the flatness $F_{u'}$ for case 2 (figure 17). Here the difference between profiles in the laminar-like and in the fully turbulent FPG boundary layer (figures 20 and 21 of Part 1) are considerable. In cases 1 and 3 there is much similarity with a ZPG boundary layer, e.g. self-similar behaviour in the sublayer and the buffer layer. In the laminar-like boundary layer of case 2 the skewness develops double troughs with $S_{u'} < 0$ and the flatness $F_{u'}$ double peaks with $F_{u'} > 0$ in a range $80 < y^+ < 800$. The second peak of $F_{u'}$ lies in the outer region of the boundary layer showing maximum values of about 19 for the ZPG-profiles which is characteristic of any turbulent boundary layer at its outer edge. The first peak reflects the highly disturbed outer region of the boundary layer with some remaining turbulent flashes in an otherwise laminar-like region.

Re_{δ_2}	862	560	420	475	1399
$S_{\tau_w'}$	0.9	1.1	3.1	2.0	1.0
$F_{\tau_w'}$	4.1	4.9	19.2	7.8	4.5

TABLE 2. Near-wall values of $S_{\tau_w'}$ and $F_{\tau_w'}$ for the profiles in figure 17.

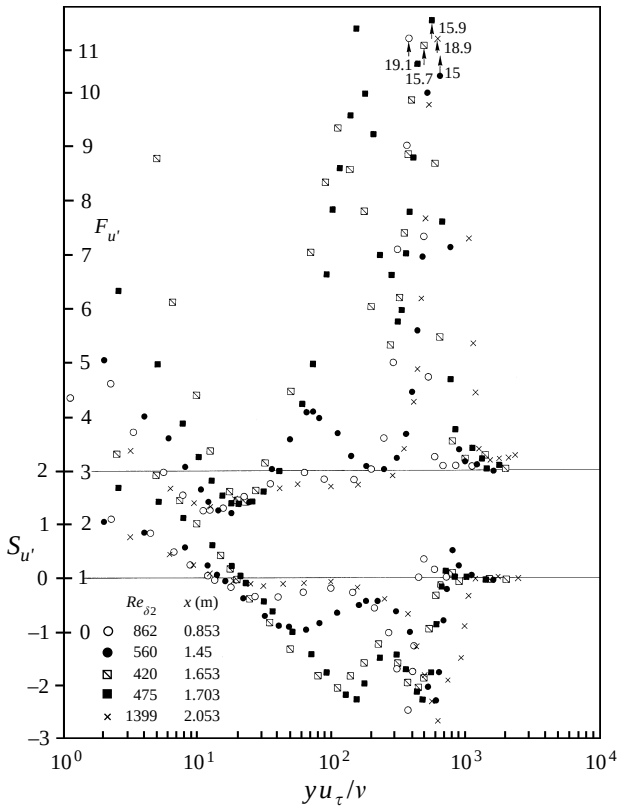

FIGURE 17. Profiles of skewness $S_{u'}$ and flatness $F_{u'}$ in a FPG turbulent boundary layer with 'relaminarization'. Case 2.

Near-wall values of $S_{\tau_w'}$ and $F_{\tau_w'}$ for the profiles of case 2 in figure 17 are given in table 2.

A comparison of the wall data for case 2 with those of case 1 (legend of figure 20, Part 1) shows that in the laminar-like state both $S_{\tau_w'}$ and $F_{\tau_w'}$ are at least twice as high in the accelerated region. The high values of $F_{\tau_w'}$ agree with the results shown as time series of τ_w' in figure 8. After retransition the Fu'- and Su'-profiles revert to their typical behaviour in a ZPG boundary layer (Fernholz & Finley 1996).

The changes in the turbulence structure due to the strongly favourable pressure gradient are also reflected in the distribution of the anisotropy parameters $(\overline{v'^2})^{1/2}/(\overline{u'^2})^{1/2}$, $(\overline{w'^2})^{1/2}/(\overline{u'^2})^{1/2}$ and of the Reynolds shear stress correlation coefficient $\overline{u'v'}/((\overline{u'^2})^{1/2}(\overline{v'^2})^{1/2})$. Figure 18 shows that the v'-anisotropy for the FPG case lies below the ZPG case (○) in the inner region with a decrease of v' due to the FPG and an increase of v' in the outer region of the boundary layer. The return to the ZPG-distribution is by no means achieved at the position of the last measured profile

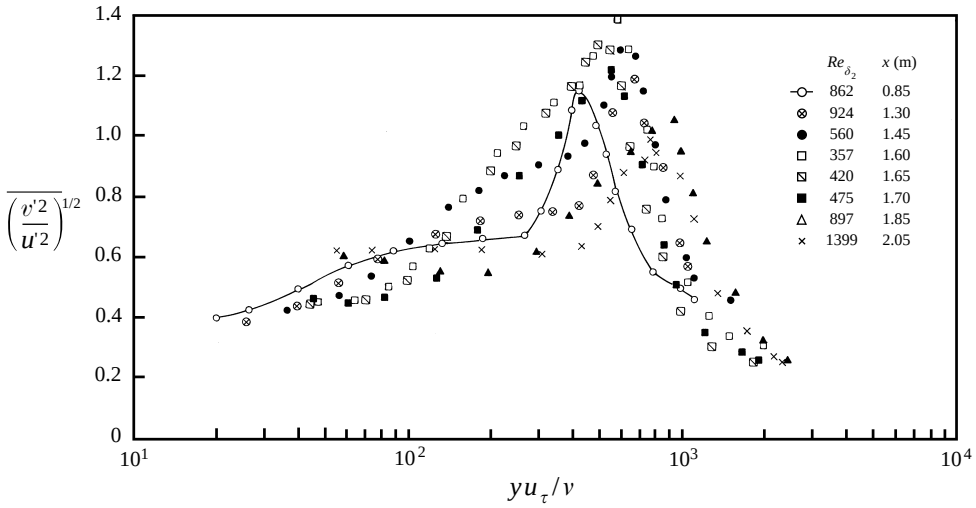

FIGURE 18. Distributions of the anisotropy parameter $(\overline{v'^2}/\overline{u'^2})^{1/2}$ in a FPG turbulent boundary layer with 'relaminarization' (case 2) (line is for visual aid only).

(×), in agreement with the slow relaxion of the outer-region turbulence structure. The peak value of the anisotropy v'/u' is reached at the position of the minimum Reynolds number (□), caused by the faster decrease of u' than of v'. Besides the effect of the FPG there is also a Reynolds number effect which makes itself felt in the shift of the peak location from about $y^+ = 600$ for the laminar-like boundary layer to $y^+ = 1600$ for the fully turbulent one (figure 22*a* of Part 1).

The w'-anisotropy distribution (figure 19) departs rather strongly from the ZPG case (□, ×). Here we find a reduction by about 30 % in the inner layer and an increase of about 100 % in the outer layer; w' receives its energy by redistribution of energy from the two other components but it is more likely that the fall in the distributions is due to the increase of u' in the near-wall region caused by the FPG. The peak values of the distributions are considerably larger than in a ZPG boundary layer in the same Reynolds number range (Fernholz & Finley 1996, their figures 63 and 65). Again the relaxation is not completed in the outer region at the last measuring station.

For a ZPG boundary layer the influence of the Reynolds number on the Reynolds shear stress correlation coefficient R_{uv} was investigated by Fernholz & Finley (1996). They found that R_{uv} varies approximately between 0.45 and 0.30 over about 90 % of the boundary layer thickness with the maximum in the outer region and the higher values at the smaller Reynolds number ($Re_{\delta_2} \leqslant 7000$). However, for a FPG boundary layer figure 20 shows the distribution of R_{uv} for case 2 with data points below the ZPG distribution (○) in the inner layer and above it in the outer layer. The maximum of R_{uv} increases with decreasing Reynolds number or increasing acceleration parameter and its location moves towards the edge of the boundary layer.

Figure 21 presents the distribution of the maxima of R_{uv} and of the structure parameter $a_1 = \overline{u'v'}/\overline{q'^2}$ against streamwise distance x, now for cases 2 and 1 for comparison. We note that both parameters begin and end with values found in ZPG boundary layers (e.g. Fernholz & Finley 1996, their figures 59 and 61) and that they rise in the acceleration region. The rise of the structure parameter a_1 is practically

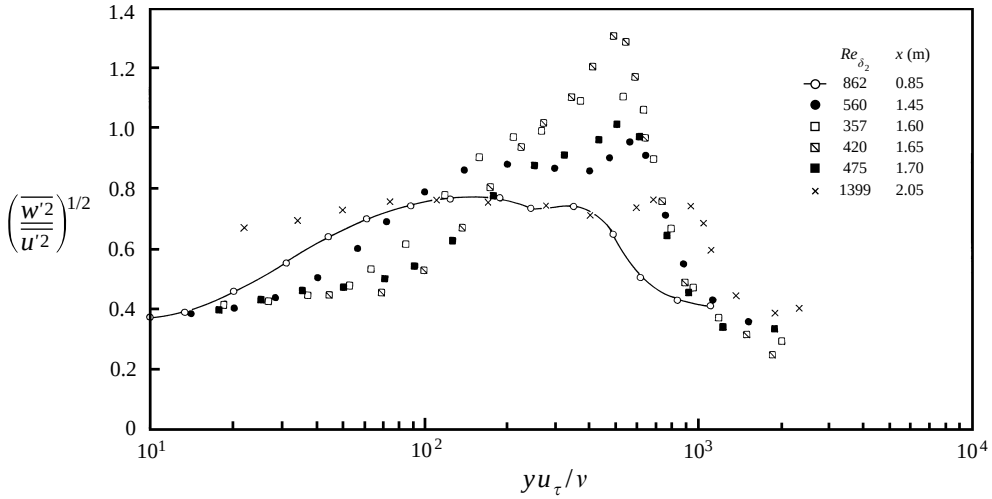

FIGURE 19. As for figure 18 but for $(\overline{w'^2}/\overline{u'^2})^{1/2}$.

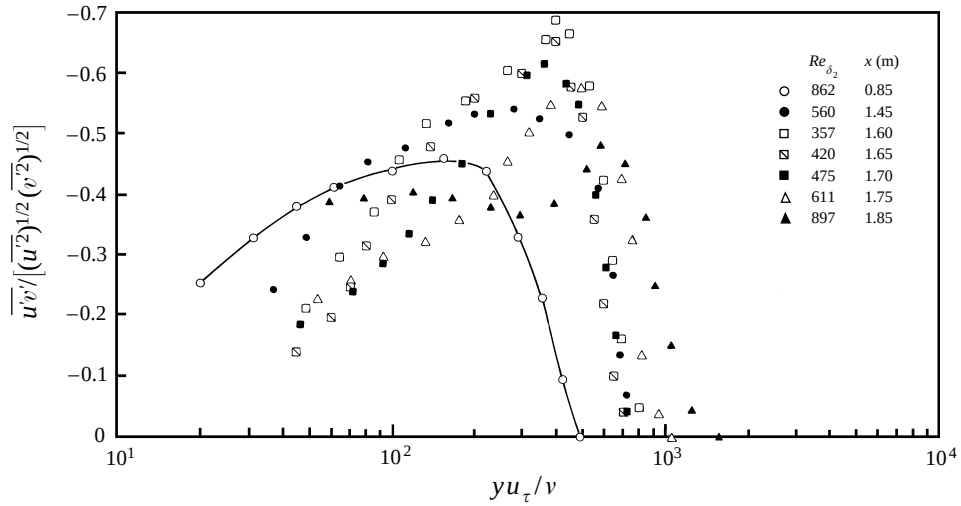

FIGURE 20. Distribution of the Reynolds shear stress correlation coefficient in a FPG turbulent boundary layer with 'relaminarization'. Case 2 (line is for visual aid only).

independent of the absolute value of the acceleration parameter K, whereas $(R_{uv})_{\max}$ increases by 20 % and 55 % for cases 1 and 2, respectively. This shows that the Reynolds shear stress decreases less than the kinetic energy $\overline{q'^2}$ in the outer region of the laminar-like boundary layer.

4. Spectra

This section presents the influence of the pressure gradient on the spectra of highly accelerated boundary layers, both fully turbulent and laminar-like. It may suffice here to record only the variation of the streamwise velocity with time at a fixed point as the field of turbulence is carried past by the mean flow with speed $\overline{u}$ (Batchelor 1967).

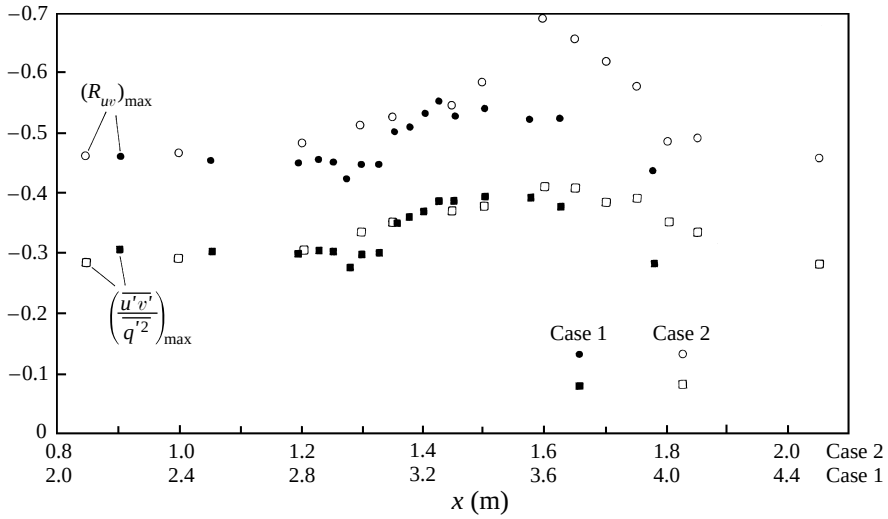

FIGURE 21. Distributions of the maxima of the Reynolds shear stress correlation coefficient R_{uv} and of the structure parameter $a_1 = -\overline{u'v'}/\overline{q'^2}$ in a FPG boundary layer without and with 'relaminarization'. Cases 1 and 2.

This yields a one-dimensional power spectral density

$$\int_0^\infty \hat{E}_1(f)\mathrm{d}f = \overline{u'^2}, \tag{4.1}$$

where f is the frequency, and in wavenumber space

$$\int_0^\infty E_{11}(k_1)\mathrm{d}k_1 = \overline{u'^2}\ . \tag{4.2}$$

The one-dimensional power spectral density $\hat{E}_1(f)$ was calculated from the linearized hot-wire data using fast-Fourier-transform routines given by Press *et al.* (1988). The first measurements of $E_1(f)$ in a FPG boundary layer were performed by Launder (1964). They show, however, only the low-frequency ranges and will be referred to in section § 5.

The longitudinal wavenumber spectrum $E_{11}(k_1)$ is usually scaled by $v_k^2\eta = (\varepsilon\nu^5)^{1/2}$ and plotted against $k_1\eta = k_1(\nu^3/\varepsilon)^{1/4}$, where η is the Kolmogorov microscale and v_k the Kolmogorov velocity, with ε the dissipation of the turbulence energy and $k_1 = 2\pi f/\overline{u}$ the wavenumber. The introduction of the wavenumber assumes that the convection velocity equals the mean velocity at the respective position in the boundary layer. This holds only for moderate turbulence levels, say $T_u < 25\,\%$, according to Bradshaw (1967) and Kim, Hussain & Moser (1987) and only for ZPG boundary layers and for channel flow. Although there is no similar investigation for accelerated boundary layers, an inspection of the present data shows that $T_u > 25\,\%$ occurs only for $y^+ \lesssim 20$ and so we have used $u_{conv} \approx \overline{u}$ for the presentation of the spectra. The part of the dissipation which can be determined from the one-dimensional spectrum is D_{11}

$$D_{11} := 2\nu \int_0^\infty k_1^2 E_{11}(k_1)\mathrm{d}k_1\ . \tag{4.3}$$

Warnack (1996) showed that without the assumption of isotropic turbulence, the longitudinal wavenumber spectrum $E_{11}(k)$ may be displayed in the following non-

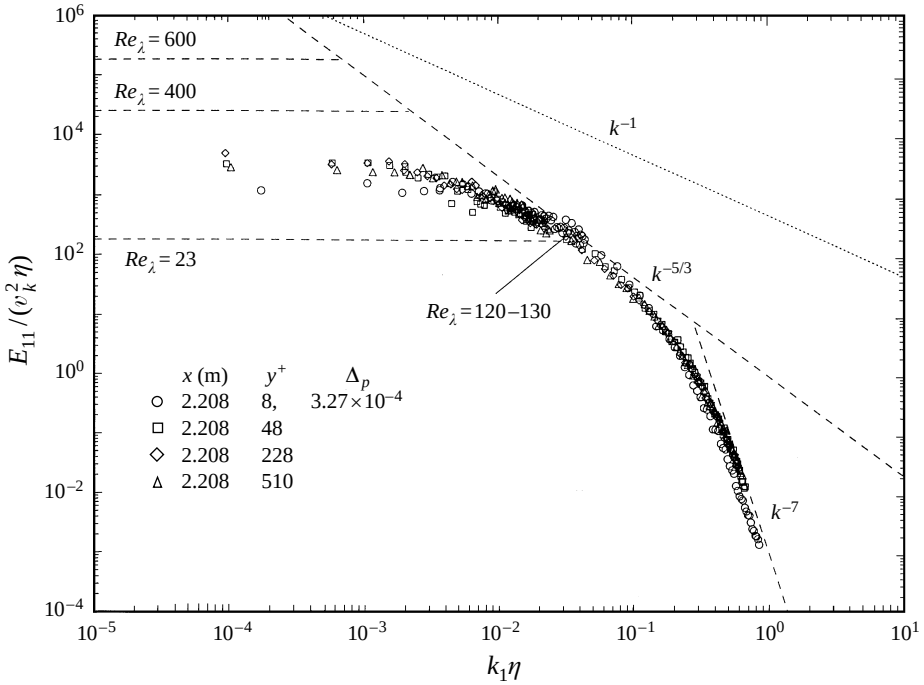

FIGURE 22. One-dimensional spectra in Kolmogorov scaling in a ZPG boundary layer at variable wall distance (y^+) and approximately constant Re_λ.

dimensional form:

$$\frac{E_{11}}{(\overline{u'^2})^{1/2}v} = F\left(\frac{kv}{(\overline{u'^2})^{1/2}}, \frac{D_{11}v}{(\overline{u'^2})^2}\right) . \tag{4.4}$$

Introducing the quantities

$$\eta := \left(\frac{v^3}{\frac{15}{2}D_{11}}\right)^{1/4}, \tag{4.5}$$

$$V_{k1} := \left(v\tfrac{15}{2}D_{11}\right)^{1/4}, \tag{4.6}$$

$$Re_\lambda := \frac{(\overline{u'^2})^{1/2}\lambda}{v} \tag{4.7}$$

into equation (4.4) yields

$$\frac{E_{11}}{v_{k1}^2\eta} = F(k\eta_1,\ Re_\lambda) \tag{4.8}$$

which reduces to the Kolmogorov representation with $\frac{15}{2}D_{11} \to \varepsilon_{isotr}$. Equation (4.8) shows that two spectra are equal if the turbulent Reynolds number is the same.

Figure 22 sets the pattern for the comparison between equation (4.8) and the measurements, showing spectra in a region with ZPG (case 1, $Re_{\delta_2} = 2549$, $x = 2.20$ m) at various values of y^+ for almost constant Re_λ ($120 \lesssim Re_\lambda \leqslant 130$). The spectra coincide well except at $y^+ = 8$ ($Tu = 33\,\%$) where the Taylor hypothesis presumably does not hold because of the high turbulence level. This and the following figures

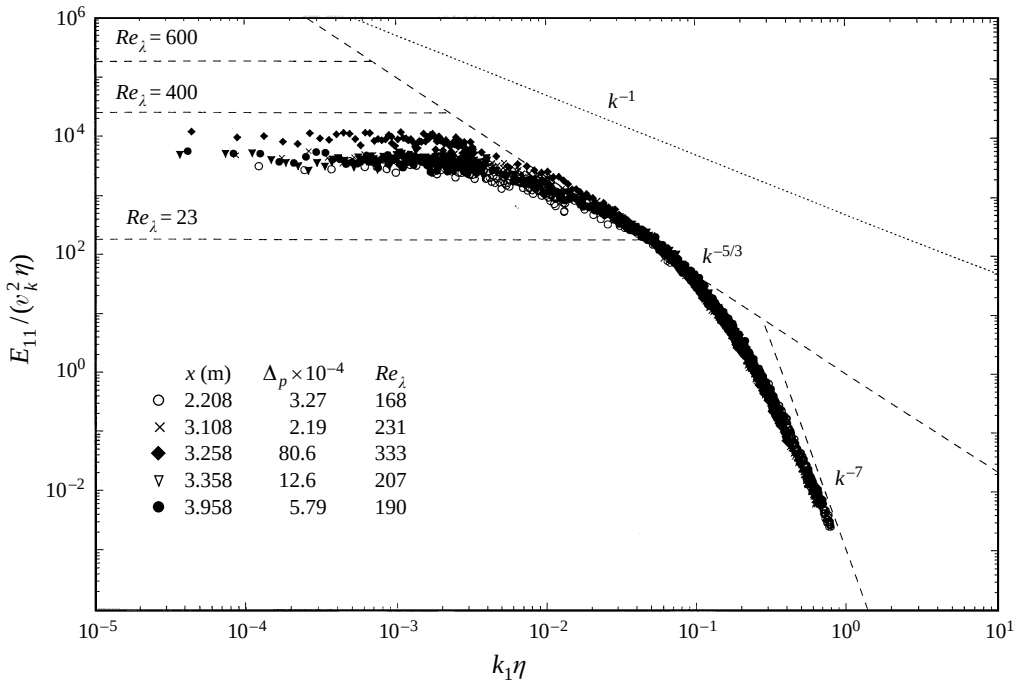

FIGURE 23. One-dimensional spectra in Kolmogorov scaling in a FPG fully turbulent boundary layer at the position where Re_λ has its maximum (case 1).

contain dashed lines which characterize the inertial subrange of the equilibrium spectrum ($E \sim k^{-5/3}$), at higher wavenumbers ($E \sim k^{-7}$), and in the lower wavenumber range ($E \sim k^{-1}$). For details see e.g. Hinze (1975). The horizontal lines serve as indicators for the influence of Re_λ and show the points where the spectra depart from the $k^{-5/3}$ behaviour for constant values of Re_λ in ZPG flows ($Re_\lambda = 23$ (Thielmann 1967); $Re_\lambda = 400$ (Sandborn & Marshall 1965); $Re_\lambda = 600$ (Saddhoughi & Veeravalli 1994)). These authors show that the energy in the low-frequency range increases with rising Re_λ.

The spectra in the accelerated fully turbulent boundary layer of case 1 follow the pattern of those in a ZPG boundary layer as is shown in figure 23. This is also true for the spectra in the initial region and in the retransition range of case 2 (figure 32). Figure 32 shows also that spectra with approximately the same value of Re_λ collapse independent of the pressure gradient as long as the acceleration is not too strong. If the profiles of case 2, however, show a laminar-like behaviour, then the spectra deviate from their universal behaviour and display no agreement with the $k^{-5/3}$ law in the region of $(Re_\lambda)_{\max}$ (figure 24). The range of approximately constant energy at low wavenumbers extends to higher wavenumbers and the level lies below the level for a ZPG boundary layer at the equivalent Re_λ.

5. Integral length scales

The behaviour of the large structures in the accelerated turbulent and laminar-like boundary layer was investigated by measuring the autocorrelation R_τ and the space

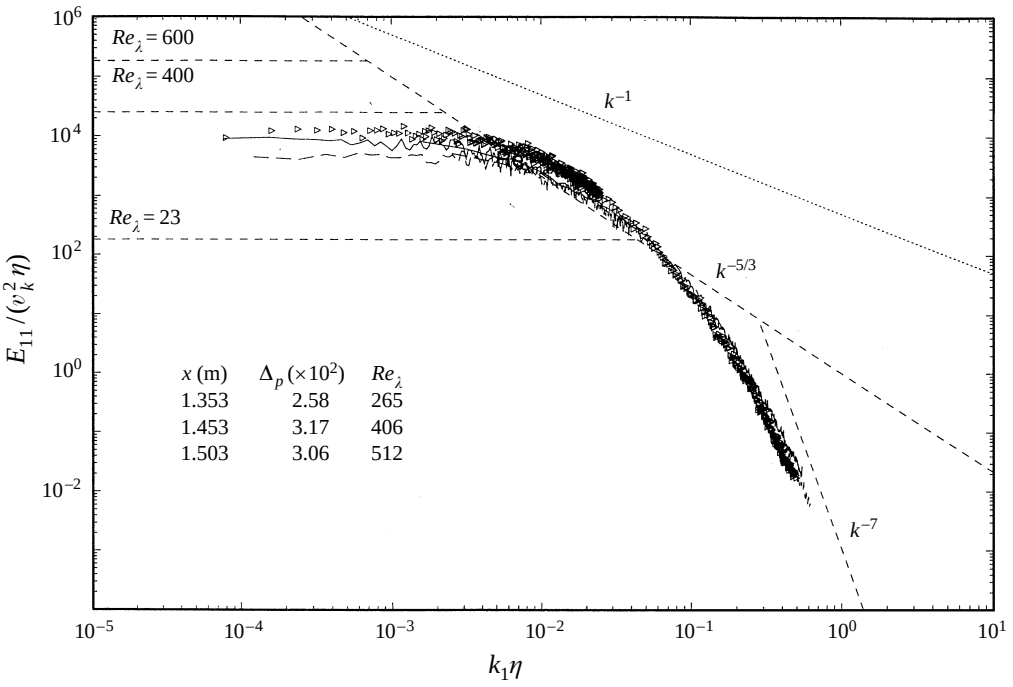

FIGURE 24. One-dimensional spectra in Kolmogorov scaling in a FPG boundary layer with laminar-like velocity profiles at the position where Re_λ has its maximum (case 2).

correlation of u' in the y-direction, $R^{\Delta y}_{u'u'}$. From these the integral length scales

$$\Lambda_\tau = \int_0^\tau R_\tau \mathrm{d}\tau, \tag{5.1}$$

$$\Lambda_y = \frac{1}{2}\int_{y-\Delta y}^{y+\Delta y} R^{\Delta y}_{u'u'}\mathrm{d}\Delta y \tag{5.2}$$

were calculated.

The development of Λ_τ and Λ_y has not been described in earlier investigations but Blackwelder & Kovasznay (1972) have measured space–time correlations of $R_{u'u'}$ and $R_{v'v'}$. These authors found that the acceleration has little effect on the correlation of the streamwise velocity component but considerable effect on the normal velocity component. These conclusions do not agree with the space correlation results of this investigation where, however, both the initial Reynolds number and the peak acceleration parameter $K_{\max}$ were lower.

For case 2, figures 25 and 26 show the profiles of $\Lambda_x = \Lambda_\tau \bar{u}$ and of Λ_y, made dimensionless by $\delta_{0.995}$. Λ_x/δ increases by up to a factor 4 in the laminar-like regime while the increase for Λ_y/δ is only by a factor 2. Λ_y was determined for $(R_{u'u'})_{\max}$ in the range $0.4 \leqslant y/\delta \leqslant 0.65$. These results show that the structures are strongly elongated in the x-direction by the acceleration. It is interesting to note that in accelerated boundary layers (case 1 is not shown here) the large-scale structures do not scale with the boundary layer thickness as they do in a ZPG or in an APG boundary layer (cf. Dengel & Fernholz 1990, their figure 18). The distributions show also that the large-scale structures at the end of the measuring region, where $\mathrm{d}p/\mathrm{d}x = 0$, still show distinct history effects (the ◆ profile differs strongly from the initial profile (○).

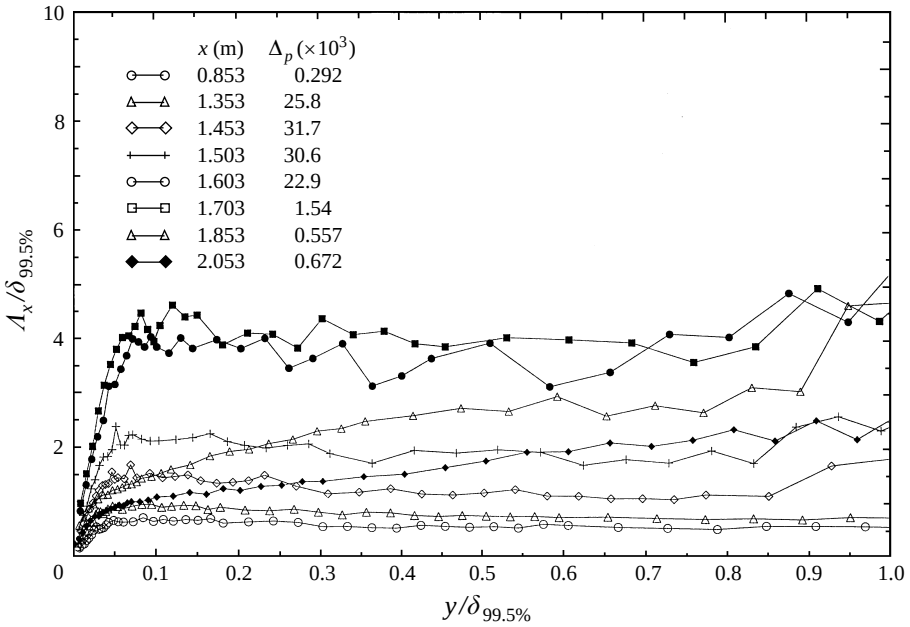

FIGURE 25. Integral length scale $\Lambda_x = \Lambda_\tau \bar{u}$ in the streamwise direction to the wall at various positions x (case 2). Lines for visual aid only.

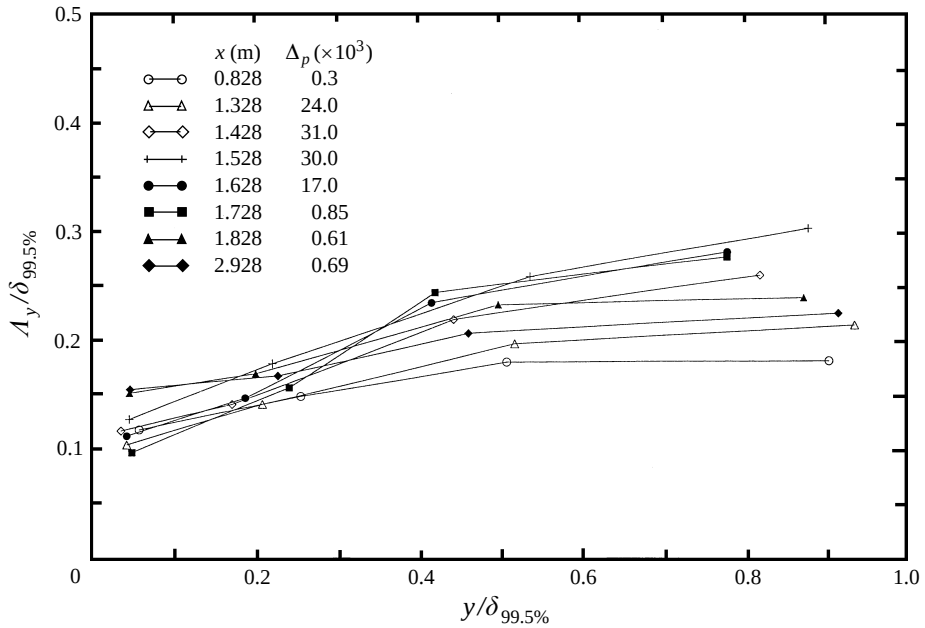

FIGURE 26. Integral length scale Λ_y in the normal direction to the wall at various positions x (case 2). Lines for visual aid only.

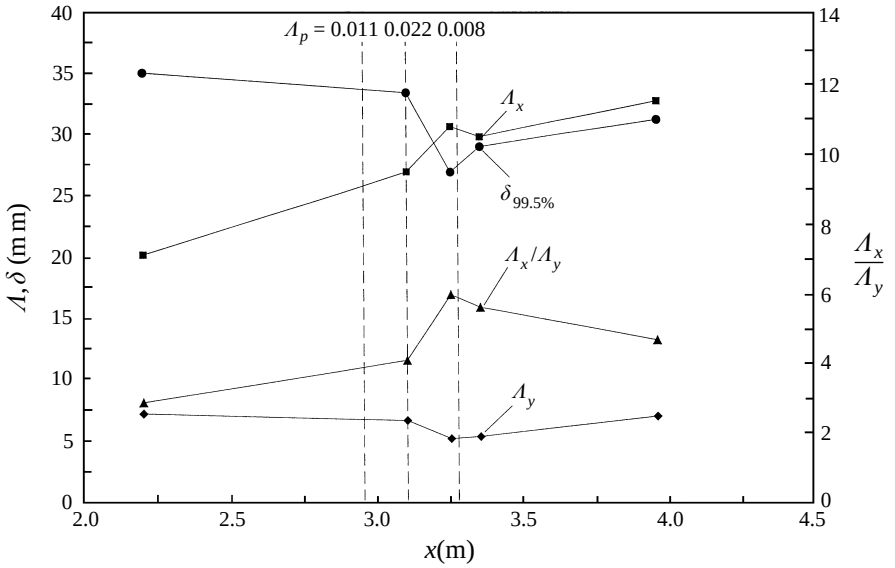

FIGURE 27. Comparion of the integral length scales Λ_x and Λ_y at $y/\delta = 0.5$ for case 1. Lines for visual aid only.

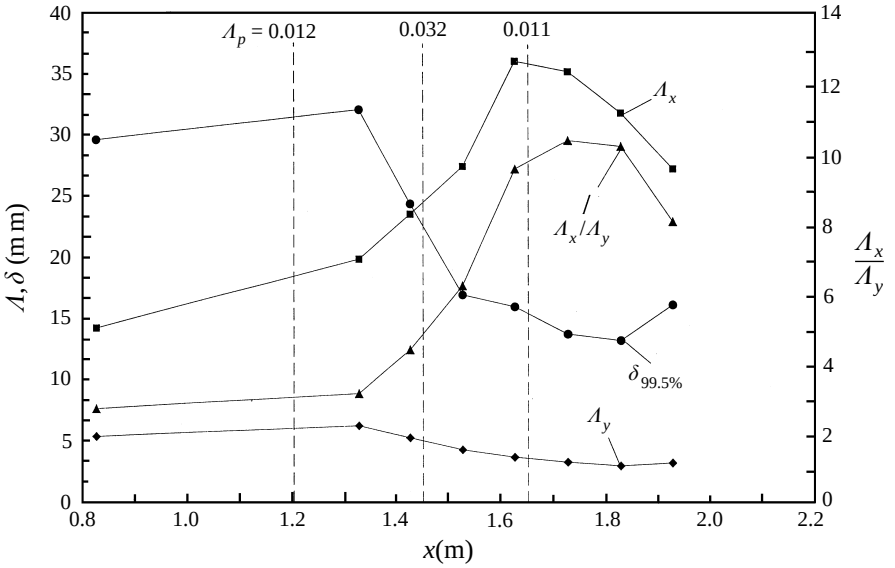

FIGURE 28. As figure 27 but for case 2.

Figures 27 and 28 compare the development of the integral length scales measured at $y/\delta \approx 0.5$ for cases 1 and 2. It is obvious that the profiles are stretched much more in the boundary layer with the higher acceleration parameter (case 2) and that the changes of Λ_x are much larger than those of Λ_y. The results for $\Lambda_x = E_{11}(0)/\overline{u'^2}$ are similar to the results of Launder (1964) who observed an energy shift towards the low-wavenumber end of the spectrum $E_{11}(k_1)/\overline{u'^2}$ through the acceleration region and thus an increase of Λ_x.

6. Discussion

Two fully turbulent boundary layers (cases 2 and 4) were exposed to a high acceleration ($K \leqslant 4 \times 10^{-6}$) in the streamwise direction with initial Reynolds numbers of 862 and 2564, respectively. The investigation showed that the pressure gradient effects were dominant and that the variation of the Reynolds number played a minor role. Consequently, it has been confirmed that relaminarization which leads to a laminar-like behaviour of mean properties of the flow, such as the mean velocity profile and the skin friction, 'is caused by the domination of pressure forces over slowly responding Reynolds stresses' (Narasimha & Sreenivasan 1973, 1979). This result excludes a parameter-connected criterion for the onset of relaminarization and for the breakdown of the standard logarithmic law (see Part 1).

Figure 3 shows that the shape parameter H_{12} and the Reynolds number Re_{δ_2} decrease and reach minima at or just downstream of the maximum of the acceleration parameter K and the maximum of c_f occurs at the location of $K_{\max}$. For values of the Falkner–Skan parameter $m = (x/u_\delta)(\mathrm{d}u_\delta/\mathrm{d}x) > 1$ the boundary layer thickness δ decreases. The mean velocity profiles reach a laminar-like state downstream of the maximum of K in the range $4 \times 10^{-6} \geqslant K \gtrsim 0$ (figures 5 and 9). In this range the shape parameter H_{12} has its maximum value and c_f its minimum which would be the case for a laminar as compared to a turbulent boundary layer. At the end of the acceleration region the boundary layer reverts quickly to a fully turbulent regime (figures 5 and 6). In both cases 2 and 4, the skin-friction velocity u_τ increases by approximately a factor of 3 within the measuring range.

Relaminarization and the laminar-like state of the boundary layer are accompanied by a significant change in the behaviour of near-wall turbulence quantities, such as $Tu_{\tau'_w}$, the skewness $S_{\tau'_w}$, the flatness $F_{\tau'_w}$ and the maximum of the Reynolds normal stress component, $(\overline{u'^2}/u_\tau^2)_{\max}$, which lies below $y^+ < 20$ (figure 7).

In the relaminarization region first the higher moments $S_{\tau'_w}$ and $F_{\tau'_w}$ and then the lower moments $(\overline{\tau'^2_w}/\bar{\tau}_w^2)^{1/2}$ and $(\overline{u'^2}/u_\tau^2)_{\max}$ reach a maximum. Skewness and flatness increase by approximately a factor of 3 compared with their initial values in the ZPG region. This increase of $F_{\tau'_w}$ is characteristic of a flow with singular high skin-friction fluctuations as displayed by the time signal of τ_w at $x = 1.653$ m presented in figure 8. The large increase of $(\overline{u'^2}/u_{\tau_{ref}}^2)_{\max}$ by a factor of 10 in the near-wall region (figure 11) is apparently characteristic of the laminar-like region just as is the decay of the normal stress in the outer region of the boundary layer (figures 11 and 12). The great 'changes' in the turbulence structure in a laminar-like boundary layer are reflected also in the profiles of the skewness S'_u and the flatness F'_u in figure 17. The specific characteristic feature is the inner peak of F'_u in the outer layer which is an indicator of large turbulent events in an otherwise laminar-like region. After retransition the F'_u- and S'_u-profiles recover fully to typical profiles in a ZPG boundary layer. The response of the Reynolds stresses to the strongly negative pressure gradient is reflected also in the profiles of the Reynolds shear stress in figures 13–15.

Qualitatively the development of the Reynolds shear stress profiles in a FPG is similar for a laminar-like and a fully turbulent boundary layer. However, the growth of the Reynolds shear stress in the outer region of the laminar-like boundary layer lags behind the skin friction and the near-wall molecular shear stress. The Reynolds stress profiles are closely connected to their respective production profiles and good qualitative agreement is seen by comparison of figures 12 and 16, for example.

A further characteristic of the turbulence in the laminar-like boundary layer is the strong increase of the anisotropy parameters $(\overline{v'^2}/\overline{u'^2})^{1/2}$ and $(\overline{w'^2}/\overline{u'^2})^{1/2}$ in the outer

region of the boundary layer (figures 18 and 19). This is due more to a decrease of $\overline{u'^2}$ and less to a change of the redistribution mechanism in the boundary layer.

In the laminar-like region of the boundary layer the spectra deviate from their universal behaviour (figure 23) and show no agreement with the $k^{-5/3}$ law near the wall. The range of approximately constant energy extends to higher wavenumbers and then falls off to approach the k^{-7} law for high values of the wavenumber k.

Although most of the Reynolds stresses have adapted to the local boundary conditions in the downstream ZPG range, neither of the integral length scales Λ_x nor Λ_y have reached their respective equilibrium values either in case 1 or in case 2 (figures 27 and 28).

The first author is grateful for the financial support by DFG and both authors for the comments by W. Debler and P. J. Finley.

REFERENCES

Badri Narayanan, M. A. & Ramjee, V. 1969 On the criteria for reverse transition in two-dimensional boundary layer flow. *J. Fluid Mech.* **35**, 225–241.

Batchelor, G. K. 1967 *Introduction to Fluid Dynamics*. Cambridge University Press.

Blackwelder, R. F. & Kovasznay, L. S. G. 1972 Large scale motion of a turbulent boundary layer during relaminarization. *J. Fluid Mech.* **53**, 61–63.

Bradshaw, P. 1967 The turbulent structure of equilibrium boundary layers. *J. Fluid Mech.* **29**, 625–646.

Dengel, P. & Fernholz, H. H. 1990 An experimental investigation of an incompressible turbulent boundary layer in the vicinity of separation. *J. Fluid Mech.* **212**, 615–636.

Erm, L. P. 1988 Low Reynolds-number turbulent boundary layers. PhD thesis, University of Melbourne.

Fernholz, H. H. & Finley, P. J. 1996 The incompressible zero-pressure-gradient turbulent boundary layer: An assessment of the data. *Prog. Aero. Sci.* **32**, 245–311.

Fernholz, H. H. & Warnack, D. 1998 The effects of a favourable pressure gradient and of the Reynolds number on an incompressible axisymmetric turbulent boundary layer. Part 1. The turbulent boundary layer. *J. Fluid Mech.* **359**, 329–356.

Hinze, J. O. 1975 *Turbulence*. McGraw–Hill.

Ichimiya, M. 1995 Properties in a relaminarizing turbulent boundary layer under a favourable pressure gradient. In *10th Symp. on Turbulent Shear Flows, Pennsylvania State University*.

Kim, H. & Hussain, F. 1993 Propagation velocity of Perturbations in turbulent channel flow. *Phys. Fluids* A **5**, 695–706.

Kim, H., Hussain, F. & Moser, R. 1987 Turbulence statistics in fully developed channel flow at low Reynolds number. *Phys. Fluids* A **5**, 133–166.

Launder, B. E. 1964 Laminarization of the turbulent boundary layer by acceleration. *MIT Gas Turbine Lab. Rep.* 77.

Loitsianski, L. G. 1972 *Laminare Grenzschichten*. Akademie Verlag, Berlin.

Narasimha, R. 1977 The three archetypes of relaminarization. *Proc. 6th Canadian Congr. Appl. Mech., Vancouver*.

Narasimha, R. 1983 Relaminarization – magnetohydrodynamics and otherwise. *Prog. Astronautics Aeronaut.* **84**, 30–52.

Narasimha, R. & Sreenivasan, K. R. 1973 Relaminarization in highly accelerated turbulent boundary layers. *J. Fluid Mech.* **61**, 417–447.

Narasimha, R. & Sreenivasan, K. R. 1979 Relaminarization of fluid flows. *Adv. Appl. Mech.* **19**, 221–309.

Patel, V. C. & Head, M. R. 1968 Reversion of turbulent to laminar flow. *J. Fluid Mech.* **34**, 371–392.

Press, W. H. & Flannery, B. P. & Teukolsky, S. A. & Vetterling, W. T. 1988 *Numerical Recipes in C*. Cambridge University Press.

Saddhoughi, S. & Veeravalli, S. 1994 Local instropy in turbulent boundary layers at high Reynolds numbers. *J. Fluid Mech.* **268**, 333–372.

Sandborn, V. A. & Marshall, R. D. 1965 Local isotropy in wind tunnel turbulence. *Colorado State Univ. Rep.* CER 65 UAS-RDM71.

Sreenivasan, K. R. 1982 Review Article: Laminarescent, relaminarizing and retransitional flows. *Acta Mech.* **44**, 1–48.

Sternberg, J. 1954 The transition from a turbulent to a laminar boundary layer. *Rep.* 906. Ballistic Res. Lab. Aberdeen.

Thielmann, H. W. 1967 Viscous region of turbulent boundary layer. *Colorado State Univ. Rep.* CER 67–68 HWT 21.

Warnack, D. 1996 Einige Eigenschaften beschleunigter turbulenter Wandgrenzschichten. Dissertation, TU Berlin.